IMA Journal of Applied Mathematics (2015) Page 1 of 23
doi:10.1093/imamat/xxx000

Interaction of in-phase and anti-phase synchronies in a coupled compartment-bulk diffusion model at a double Hopf bifurcation

JIA GOU
Department of Mathematics, Univ. of British Columbia, Vancouver, BC, Canada V6T 1Z2

YUE-XIAN LI
Department of Mathematics, Univ. of British Columbia, Vancouver, BC, Canada V6T 1Z2
Department of Zoology, Univ. of British Columbia, Vancouver, BC, Canada V6T 1Z4

AND

WAYNE NAGATA*
Department of Mathematics, Univ. of British Columbia, Vancouver, BC, Canada V6T 1Z2
*Corresponding author: nagata@math.ubc.ca

[Received on 17 July 2015]

We study a model of chemical oscillations in two identical compartments, coupled by a chemical signal diffusing and degrading in the one-dimensional bulk medium between the compartments. The nonlinear compartment-bulk diffusion model consists of a coupled system of ordinary and partial differential equations. Previous numerical work on this system reveals the presence of two modes of synchronized oscillations, in-phase and anti-phase, which arise from Hopf bifurcations of the unique steady state of the system. The coincidence of the two Hopf bifurcations indicates a double Hopf bifurcation point. We use center manifold and normal form theory to reduce the local dynamics of the model system to a system of two amplitude equations, which determines the patterns of Hopf bifurcation and stability of the two modes near the double Hopf point. In the case of bistability, the stable manifold of an unstable invariant torus forms the boundary between the basins of attraction of the stable in-phase and anti-phase modes. Numerical simulations support these predictions.

Keywords: Synchrony, coupled oscillators, bulk diffusion coupling, double Hopf bifurcation

1. Introduction

Communication is crucial for a group of individuals to accomplish cooperative activities such as synchrony. In neuronal systems, synchrony between different regions of the brain, communicating through synaptic connections, is thought to be the basis of many cognitive activities (Varela et al., 2001). Between individual cells, there are numerous examples of synchrony, such as glycolytic oscillations in yeast cells (De Monte et al., 2007), pulsatile secretion of insulin in pancreatic β cells (MacDonald & Rorsman, 2006), and cell cycles in colonies of amoebae (Segota et al., 2014). Among a variety of communication methods between cells such as synaptic connections or gap junctions, here we are interested in the case where individual cells secrete a signalling chemical into the extracellular space, or bulk region, where it diffuses and is detected by other cells, which can result in the entire population of cells switching collectively to a synchronized dynamical behaviour. This occurs, for example, in quorum sensing (Chiang et al., 2011; Miller & Bassler, 2001; Müller et al., 2006; Müller & Uecker, 2013).

One biological phenomenon we are motivated by is the synchronized rhythmic secretion of gonado-

tropin-releasing hormone (GnRH) from neuron cells in the hypothalamus region of the mammalian brain. This periodic signal has been shown to be crucial in maintaining the normal reproductive activities in rhesus monkeys (Knobil, 1974). Experiments have shown that some 800 to 2000 GnRH neurons are scattered in a few areas of hypothalamus. In order to generate an overall rhythmic GnRH pattern, synchronization in the secretory activities of the neurons is essential. A synchronization mechanism was proposed by Li & Khadra (2008), where it was assumed the neurons are coupled through GnRH secreted into the extracellular space. The predictions of this model were shown to be consistent with *in vivo* experiments. However, this model assumed the extracellular space was continuously stirred so that GnRH is diluted and averaged immediately. A more realistic model in the absence of stirring would consider the diffusion of GnRH in the bulk region.

A chemical concentration in the space between biological cells can be modeled by a bulk diffusion field, and the chemical reactions in the cells themselves modeled by systems of ordinary differential equations (or integro-differential equations, etc.) evolving in spatially isolated compartments that are coupled by a one or more partial differential equations for diffusion in the bulk. A well known application of this type of model considers the triggering of aggregation of slime mold amoebae *Dictyostelium discoideum* when the chemical cAMP is secreted by the amoebae into the bulk region, e.g. (Goldbeter, 1990). Bulk diffusion of signalling chemicals within the cytoplasm of a cell has also been considered, e.g. (Busenberg & Mahaffy, 1985). In quorum sensing, coupling compartments with bulk diffusion can have important theoretical effects (Müller et al., 2006), such as providing dissipation that allows approximation methods to be used to determine long-term dynamics (Müller & Uecker, 2013). In other applications of coupled compartment-bulk diffusion models, the compartments can instead correspond to dynamically active membranes, such as in systems of membranes and chemicals within a cell (Gomez-Marin et al., 2007), cell membranes and viruses (Chou & D'Orsogna, 2007), or chemically active surfaces and catalysts (Shvartsman et al., 1999).

In recent work (Gou et al., 2015a), a coupled compartment-bulk diffusion model with a one-dimensional domain was studied. Identical chemical oscillators in two compartments are coupled with a scalar field that diffuses and degrades in the bulk region. Simulations show that the coupled compartment-bulk system can have two different modes of synchronized oscillations, or synchrony: an in-phase (or synchronous) mode, where the two compartments oscillate at identical frequencies with no phase difference between them, and an anti-phase (or asynchronous) mode, where the two compartments oscillate at identical frequencies with a phase difference of half a period. Parameter studies using numerical bifurcation and continuation methods on spatially discretized approximations of the system show that the two modes of synchrony arise from Hopf bifurcations, and there are parameter regions where bistability occurs, where both modes of synchrony exist and both are stable. These studies show there are double Hopf (or Hopf-Hopf) points, parameter values where the Hopf bifurcations of the in-phase and anti-phase modes coincide. At such points, the interaction of the in-phase and anti-phase synchronies can be studied analytically, without spatial discretization.

Following from observations made in the parameter study of the spatially discretized system, in this paper we analyze a double Hopf bifurcation in the continuum compartment-bulk system. The analysis explains and predicts certain features of the parameter study of the system regarding the interaction of in-phase and anti-phase modes. For example, in parameter regions of bistability near the double Hopf point, there is an unstable invariant torus in the dynamics whose stable manifold forms a boundary in phase space between the stable in-phase and anti-phase modes. We express the coupled compartment-bulk system as an evolution equation in an infinite-dimensional space, and use center manifold theory to reduce the evolution to a four-dimensional local invariant manifold in the infinite-dimensional space. This latter evolution is further reduced to a normal form, which is then used to make predictions about

the in-phase and anti-phase modes and their nonlinear interaction near the double Hopf bifurcation. In the following section, we give the model system, that describes the two diffusively coupled cells. Then in section 3 we find in parameter space the location of the double Hopf point, and calculate associated eigenvalues and eigenvectors. In section 4 we describe the double Hopf bifurcation analysis and its results, and describe tests of its predictions using AUTO and simulations. We conclude the paper with a discussion.

2. The coupled compartment-bulk diffusion model

The model we consider describes chemical reactions in two spatially separated compartments, coupled by the diffusion and degradation of a signalling chemical in the bulk medium between the compartments. The compartments may be regarded as biological cells, or as dynamically active membbranes, which can interact with a signalling chemical in the bulk. We take a one-dimensional bulk medium, represented by a bounded interval whose endpoints represent the two compartments. The concentration of the signalling chemical in the bulk is represented by a scalar field which satifies a linear partial differential equation (PDE) for diffusion and degradation, and interacts with the compartments through flux boundary conditions. The chemical reactions in the compartments are represented by nonlinear systems of ordinary differential equations (ODEs) for each compartment, thus the compartment-bulk model is a coupled PDE-ODE system.

We represent the bulk region by the interval $[-L,+L]$, where $L>0$ is a constant. Let $C(x,t)$ denote the concentration of the signalling chemical in the bulk at location x in the interval, at time t. We model the diffusion and degradation of the signalling chemical in the bulk with the linear PDE

$$\frac{\partial C}{\partial t} = D\frac{\partial^2 C}{\partial x^2} - kC, \qquad -L<x<+L, \quad t>0, \tag{2.1}$$

where $D>0$ and $k>0$ are diffusion and degradation constants.

Two compartments are represented by the boundaries of the interval $x=-L$ and $x=+L$. Let $V_-(t)$ and $V_+(t)$ denote the concentration of the signalling chemical in the compartment at $x=-L$ and at $x=+L$, respectively. We assume the efflux of the signalling chemical from each compartment is proportional to the difference between the concentration inside each compartment and the concentration outside of it in the bulk, with the influence of each compartment on the bulk given by linear flux boundary conditions

$$\begin{aligned} -D\frac{\partial C}{\partial x}(-L,t) &= \kappa\left[V_-(t)-C(-L,t)\right], \\ +D\frac{\partial C}{\partial x}(+L,t) &= \kappa\left[V_+(t)-C(+L,t)\right], \end{aligned} \tag{2.2}$$

where κ is a positive flux constant. Thus, if the concentration $V_\pm(t)$ of the signalling chemical inside a compartment is higher than the concentration $C(\pm L,t)$ at the corresponding boundary of the bulk region, there is a positive flux of the chemical out of the compartment, into the bulk.

Inside each compartment, at $x=-L$ and at $x=+L$, the signalling chemical reacts with some intermediate chemical product, whose concentrations are denoted $W_-(t)$ and $W_+(t)$, respectively. The reactions are governed by ordinary differential equations

$$\begin{aligned} \frac{dV_-}{dt} &= f(V_-,W_-)+\beta\left[C(-L,\cdot)-V_-\right], \\ \frac{dW_-}{dt} &= g(V_-,\,W_-), \end{aligned} \tag{2.3}$$

inside the compartment at $x = -L$, and

$$\begin{aligned} \frac{dV_+}{dt} &= f(V_+, W_+) + \beta\,[C(+L,\cdot) - V_+]\,, \\ \frac{dW_+}{dt} &= g(V_+,\, W_+), \end{aligned} \tag{2.4}$$

inside the compartment at $x = +L$. The influence of the outside bulk concentration of the signalling chemical on the reaction dynamics inside each compartment is described by the coupling terms $\beta[C(\pm L,\cdot) - V_\pm]$, with a positive constant β that represents the coupling strength.

We take identical compartments, so κ and β are the same for each compartment, and the functions f and g representing the reaction kinetics inside each compartment are the same. For specific kinetics, we take the Sel'kov model, originally used to describe glycolysis

$$\begin{aligned} f(V,\, W) &= -V + \alpha W + V^2 W, \\ g(V,\, W) &= \varepsilon(\mu - \alpha W - V^2 W), \end{aligned} \tag{2.5}$$

where ε, α and μ are positive constants. These kinetics have the property that when the compartments are uncoupled ($\beta = 0$) there is a unique steady state $V_0 = \mu$, $W_0 = \mu/(\alpha + V_0^2)$. For some parameter values this steady state is globally asymptotically stable, while for other parameter values the steady state is unstable and there is a unique stable limit cycle.

Our model system is (2.1)–(2.5), which in more mathematical terms can be described as a pair of identical conditional oscillators, coupled by bulk diffusion. The choice of Sel'kov kinetics is not essential: qualitatively similar results for the model have been found using other kinetics (Gou & Ward, 2015). Since the cells are identical, the model system (2.1)–(2.5) has a reflection symmetry, under spatial reflection of the bulk region $x \to -x$ and exchange of the compartments.

3. Linearized stability and numerical bifurcation results

In this section we study the eigenvalue problem that gives the linearized stability of the steady state solution of the model system. From this we obtain parameter values that give Hopf points for two types of marginally stable synchronized linear oscillations, called anti-phase (asynchronous) and in-phase (synchronous) eigenvectors. In particular, we obtain parameter values for a double Hopf point, where both the anti-phase and in-phase eigenvectors are marginally stable. We also describe results of numerical studies of stability and bifurcation.

We find the steady state, or equilibrium, of the model system (2.1)–(2.5) as

$$C(x,\, t) = C^e(x), \quad V_-(t) = V^e, \quad V_+(t) = V^e, \quad W_-(t) = W^e, \quad W_+(t) = W^e, \tag{3.1}$$

where

$$C^e(x) = C_0^e \frac{\cosh(\Omega_0 x)}{\cosh(\Omega_0 L)}, \quad V^e = \frac{\mu + \beta C_0^e}{1+\beta}, \quad W^e = \frac{\mu}{1 + (V^e)^2},$$

and

$$\Omega_0 = \sqrt{\frac{k}{D}}, \quad C_0^e = \frac{\kappa\mu}{\kappa + D\Omega_0(1+\beta)\tanh(\Omega_0 L)}.$$

We note that the steady state is even with respect to the reflection symmetry. Then defining deviations from the steady state by

$$C(x,\, t) = C^e(x) + c(x,\, t), \quad V_\pm(t) = V^e + v_\pm(t), \quad W_\pm(t) = W^e + w_\pm(t),$$

from (2.1)–(2.4) we obtain the corresponding differential equations for the deviations

$$\begin{aligned}
\frac{\partial c}{\partial t} &= D\frac{\partial^2 c}{\partial x^2} - kc,\\
\frac{dv_-}{dt} &= f(V^e+v_-,W^e+w_-) - f(V^e,W^e) + \beta\left[c(-L,\cdot) - v_-\right],\\
\frac{dw_-}{dt} &= g(V^e+v_-,W^e+w_-) - g(V^e,W^e),\\
\frac{dv_+}{dt} &= f(V^e+v_+,W^e+w_+) - f(V^e,W^e) + \beta\left[c(+L,\cdot) - v_+\right],\\
\frac{dw_+}{dt} &= g(V^e+v_+,W^e+w_+) - g(V^e,W^e),
\end{aligned} \tag{3.2}$$

with boundary conditions

$$\begin{aligned}
-D\frac{\partial c}{\partial x}(-L,\cdot) &= \kappa\left[v_- - c(-L,\cdot)\right],\\
+D\frac{\partial c}{\partial x}(+L,\cdot) &= \kappa\left[v_+ - c(+L,\cdot)\right],
\end{aligned} \tag{3.3}$$

We linearize (3.2)–(3.3) about the origin (which now corresponds to the steady state) and obtain

$$\begin{aligned}
\frac{\partial c}{\partial t} &= D\frac{\partial^2 c}{\partial x^2} - kc,\\
\frac{dv_\pm}{dt} &= f_V^e v_\pm + f_W^e w_\pm + \beta\left[c(\pm L,\cdot) - v_\pm\right],\\
\frac{dw_\pm}{dt} &= g_V^e v_\pm + g_W^e w_\pm,
\end{aligned} \tag{3.4}$$

with the same boundary conditions

$$\pm D\frac{\partial c}{\partial x}(\pm L,\cdot) = \kappa\left[v_\pm - c(\pm L,\cdot)\right], \tag{3.5}$$

where f_V^e, g_V^e f_W^e and g_W^e are the partial derivatives of f and g, evaluated at the steady state (3.1).

To study the linearized stability of the steady state, we make the usual ansatz $c(x,t) = e^{\lambda t}\eta(x)$, $v_\pm = e^{\lambda t}\varphi_\pm$ and $w_\pm = e^{\lambda t}\psi_\pm$ in (3.4)–(3.5), and obtain the eigenvalue problem

$$\begin{aligned}
\lambda\eta &= D\eta'' - k\eta,\\
\lambda\varphi_\pm &= f_V^e\varphi_\pm + f_W^e\psi_\pm + \beta\left[\eta(\pm L) - \varphi_\pm\right],\\
\lambda\psi_\pm &= \varepsilon[g_V^e\varphi_\pm + g_W^e\psi_\pm],
\end{aligned} \tag{3.6}$$

with boundary conditions

$$\pm D\eta'(\pm L) = \kappa\left[\varphi_\pm - \eta(\pm L)\right]. \tag{3.7}$$

If $\operatorname{Re}\lambda < 0$ for all eigenvalues λ, then the steady state is asymptotically stable. We seek parameter values where the steady state is marginally stable: $\operatorname{Re}\lambda = 0$ for finitely many eigenvalues, called critical eigenvalues, and $\operatorname{Re}\lambda < 0$ for all remaining eigenvalues. Near such parameter values, we expect the

nonlinear system (3.2)–(3.3) will have bifurcations of solutions near the steady state. Because of the oscillatory nature of the reaction kinetics, at parameter values where the steady state is marginally stable, the critical eigenvalues are purely imaginary

$$\lambda = i\omega$$

and we expect Hopf bifurcations in the nonlinear system at the corresponding parameter values. We call the parameter values corresponding to marginal stability with purely imaginary eigenvalues Hopf points.

Due to the reflection symmetry of (3.6)–(3.7), the eigenvectors come in two types, odd, or "anti-phase" (or "asynchronous"), with

$$\eta(-x) = -\eta(x), \quad v_- = -v_+, \quad w_- = -w_+,$$

and even, or "in-phase" (or "synchronous"), with

$$\eta(-x) = \eta(x), \quad v_- = v_+, \quad w_- = w_+,$$

Solving the eigenvalue problem for anti-phase eigenvectors, we have

$$\eta_-(x) = \eta_1^0 \frac{\sinh(\Omega_\lambda x)}{\sinh(\Omega_\lambda L)}$$

for some constant η_1^0, where

$$\Omega_\lambda = \sqrt{\frac{k+\lambda}{D}},$$

using the principal branch of the square root so that Ω_λ is analytic in $\mathrm{Re}\,\lambda > -k$, and the boundary condition at $x = +L$ gives

$$[\kappa + D\Omega_\lambda \coth(\Omega_\lambda L)]\eta_1^0 = \kappa\varphi_-.$$

Therefore the φ_- and ψ_- components of an anti-phase eigenvector satisfy the homogeneous system of linear equations

$$\begin{aligned} [f_V^e - p_-(\lambda) - \lambda]\varphi_- + f_W^e \psi_- &= 0, \\ g_V^e \varphi_- + (g_W^e - \lambda)\psi_- &= 0, \end{aligned} \tag{3.8}$$

where

$$p_-(\lambda) = \frac{D\Omega_\lambda \coth(\Omega_\lambda L)}{\kappa + D\Omega_\lambda \coth(\Omega_\lambda L)}.$$

Taking the determinant of the coefficient matrix of (3.8) we obtain a transcendental equation for any eigenvalue λ for anti-phase eigenvectors

$$[f_V^e - p_-(\lambda) - \lambda](g_W^e - \lambda) - f_W^e g_V^e = 0. \tag{3.9}$$

Similarly, for in-phase eigenvectors we have

$$\eta_+(x) = \eta_+^0 \frac{\cosh(\Omega_\lambda x)}{\cosh(\Omega_\lambda L)}$$

and λ must satisfy

$$[f_V^e - p_+(\lambda) - \lambda](g_W^e - \lambda) - f_W^e g_V^e = 0, \tag{3.10}$$

where

$$p_+(\lambda) = \frac{D\Omega_\lambda \tanh(\Omega_\lambda L)}{\kappa + D\Omega_\lambda \tanh(\Omega_\lambda L)}.$$

To study instabilities of the steady state, we determine the number of roots λ of (3.9) and (3.10) and their distribution in the complex λ-plane. In (Gou et al., 2015a), a winding number criterion is numerically implemented. Also, the system is spatially discretized with finite differences and the path-continuation and bifurcation program AUTO (Doedel et al., 1997) is used, with the convenient interface provided by the dynamical systems software package XPPAUT (Ermentrout, 2002), to study different types of instabilities and dynamical behavior.

The use of AUTO confirms, at least for spatially discretized approximations, that Hopf points indeed correspond to Hopf bifurcations of nonlinear periodic in-phase and anti-phase modes of synchrony. The linear stability of the nonlinear periodic modes is also studied with AUTO, see Gou et al. (2015a). We note the computations show bistability in some parameter regions, where both modes of synchrony are stable. It is also found that modes can lose stability as a conjugate pair of Floquet multipliers move out of the unit circle in the complex plane, typically associated with a torus bifurcation. Furthermore, in simulations of the system with initial conditions nearly corresponding to an anti-phase mode but with parameters such that only the in-phase mode is stable, the solution rotates in phase space for some time before it settles down to a stable in-phase mode. These observations lead us to suspect the existence of unstable torus (or quasiperiodic, or modulated wave) solutions. All of these phenomena could be found near a double Hopf point, parameter values where the marginal stability curves of Hopf points for the in-phase and anti-phase modes intersect.

There appear to be infinitely many double Hopf points in parameter space, for example as L increases without bound, but many of the intersections of the anti-phase and in-phase marginal stability curves are close to degenerate. At any sufficiently nondegenerate double Hopf point, we can accurately find numerical values for the parameters at the point, by solving the eigenvalue equations (3.9) and (3.10). For example, we fix parameter values at

$$\mu = 2, \quad \alpha = 0.9, \quad \varepsilon = 0.15, \quad \kappa = 1, \quad k = 1, \quad L = 1, \tag{3.11}$$

then with β and D as free parameters, we use the mathematical software package Maple to solve (3.9) for a purely imaginary eigenvalue

$$\lambda = i\omega_1$$

to find a nmarginal stability curve of Hopf points in the βD-plane for anti-phase eigenvectors. Similarly, we solve (3.10) with

$$\lambda = i\omega_2$$

to obtain another marginal stability curve of Hopf points for in-phase eigenvectors. Figure 1 shows marginal stability curves of Hopf points obtained by solving (3.9) and (3.10) with parameter values (3.11). For (β, D) values along the red dashed curve, the steady state is marginally stable to an anti-phase eigenvector, while along the blue solid curve it is marginally stable to an in-phase eigenvector. These curves intersect at double Hopf points, which can be found numerically by simultaneously solving (3.9) and (3.10). We obtain, for the leftmost double Hopf point seen in Figure 1, parameter values

$$\beta = 0.508394 \quad D = 0.555509, \tag{3.12}$$

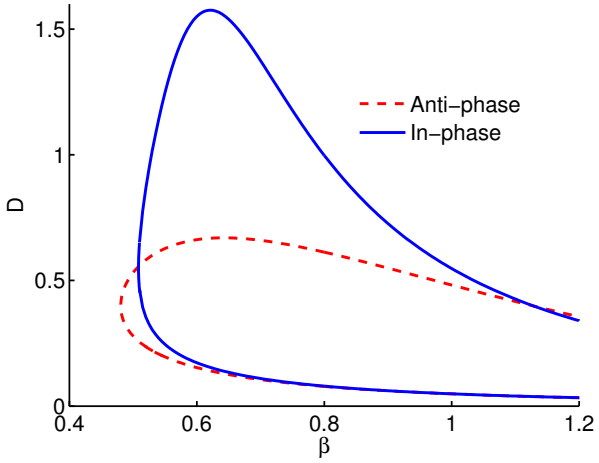

FIG. 1. Marginal stability curves for parameter values (3.11). Both marginal stability curves consist of Hopf points for anti-phase (red dashed curve) or in-phase (blue solid curve) eigenvectors. The two curves intersect at double Hopf points.

with

$$\omega_1 = 0.811618, \quad \omega_2 = 0.794334.$$

We check, using spatially discretized finite-difference approximations of the eigenvalue problem (3.6)–(3.7), for parameter values at the double Hopf point (3.11)–(3.12), that (allowing for small discretization errors) there are four critical, purely imaginary simple eigenvalues $\lambda = \pm i\omega_{1,2}$, and all the remaining eigenvalues have negative real parts bounded away from 0.

If parameters are varied continuously, the eigenvalues change continuously. Therefore, if parameters are near the double Hopf point, there are four simple eigenvalues near $\pm i\omega_{1,2}$, near the imaginary axis, which we still call critical eigenvalues, and the remaining eigenvalues still have negative real parts bounded away from 0.

We conclude this section by introducing a vector notation, which makes the subsequent bifurcation calculations more convenient. We let

$$X(t) = \begin{bmatrix} c(x,t) \\ v_-(t) \\ w_-(t) \\ v_+(t) \\ w_+(t) \end{bmatrix}, \tag{3.13}$$

where for each t, $X(t)$ belongs to a real infinite-dimensional function space H consisting of vectors $X(t)$ whose components satisfy the boundary conditions (3.5). We define the linear differential operator M

by

$$MX = \begin{bmatrix} D\frac{\partial^2 c}{\partial x^2} - kc \\ f_V^e v_- + f_W^e w_- + \beta[c(-L,\cdot) - v_-] \\ g_V^e v_- + g_W^e w_- \\ f_V^e v_+ + f_W^e w_+ \beta[c(+L,\cdot) - v_+] \\ g_V^e v_+ + g_W^e w_+ \end{bmatrix}, \tag{3.14}$$

for all $X(t)$ belonging to H. Then the linearized system (3.4)–(3.5) can be written as

$$\dot{X} = MX, \tag{3.15}$$

for $X(t)$ belonging to H, where the dot denotes differentiation with respect to t. Setting $X(t) = e^{\lambda t} q$, where

$$q = \begin{bmatrix} \eta(x) \\ \varphi_- \\ \psi_- \\ \varphi_+ \\ \psi_+ \end{bmatrix}$$

belongs to H, the eigenvalue problem (3.6)–(3.7) is expressed as

$$Mq = \lambda q, \tag{3.16}$$

For complex eigenvalues λ, we seek the corresponding eigenvectors q in the complexification of H. In particular, at the double Hopf point (3.11)–(3.12) we have

$$Mq_1 = i\omega_1 q_1, \quad Mq_2 = i\omega_2 q_2.$$

The complex eigenvectors (up to multiplication by an arbitrary complex scalar) are

$$q_1 = \begin{bmatrix} \eta_1^0 \sinh(\Omega_1 x)/\sinh(\Omega_1 L) \\ -1 \\ -g_V^e/(i\omega_1 - g_W^e) \\ 1 \\ g_V^e/(i\omega_1 - g_W^e) \end{bmatrix}, \quad q_2 = \begin{bmatrix} \eta_2^0 \cosh(\Omega_2 x)/\cosh(\Omega_2 L) \\ 1 \\ g_V^e/(i\omega_2 - g_W^e) \\ 1 \\ g_V^e/(i\omega_2 - g_W^e) \end{bmatrix}, \tag{3.17}$$

where

$$\Omega_1 = \sqrt{\tfrac{k+i\omega_1}{D}}, \quad \Omega_2 = \sqrt{\tfrac{k+i\omega_2}{D}}, \quad \eta_1^0 = \tfrac{\kappa}{\kappa + D\Omega_1 \coth(\Omega_1 L)}, \quad \eta_2^0 = \tfrac{\kappa}{\kappa + D\Omega_2 \coth(\Omega_2 L)}.$$

Generally, the critical eigenspace (or center subspace) T^c is the real subspace consisting of the span of the real and imaginary parts of the (generalized) eigenvectors corresponding to all eigenvalues λ with $\operatorname{Re}\lambda = 0$. In our specific case it is the four-dimensional subspace

$$T^c = \operatorname{span}\{\operatorname{Re} q_1, \operatorname{Im} q_1, \operatorname{Re} q_2, \operatorname{Im} q_2\}.$$

For later computational convenience we express the critical eigenspace in complex notation as

$$T^c = \{z_1 q_1 + \bar{z}_1 \bar{q}_1 + z_2 q_2 + \bar{z}_2 \bar{q}_2 : z_1, z_2 \in \mathbb{C}\}.$$

Since all eigenvalues other than the four critical ones $\pm i\omega_{1,2}$ have negative real parts, the complementary subspace to T^c in H is T^s, the infinite-dimensional stable subspace.

4. Double Hopf bifurcation

In the previous section, we show there are double Hopf points, i.e. parameter values where the critical eigenvalues for the linearization of the model system are two pairs of purely imaginary eigenvalues $\pm i\omega_1$, $\pm i\omega_2$. In the nonlinear model system itself, for parameter values near the double Hopf point, we expect bifurcations of nonlinear modes of synchronized oscillations that resemble the linear anti-phase and in-phase eigenvectors. This is confirmed by a bifurcation analysis, which also tells us the stabilities of the nonlinear anti-phase and in-phase modes, and how the modes interact near the double Hopf point. Key to this analysis is the reduction of the infinite-dimensional model system near the steady state to a four-dimensional normal form.

We extend the vector notation introduced in the previous section to the nonlinear problem, and write the model system (2.1)–(2.5) as

$$\dot{X} = MX + \tfrac{1}{2!}B(X,X) + \tfrac{1}{3!}C(X,X,X), \tag{4.1}$$

for $X(t)$ belonging to H, where $X(t)$ is given by (3.13) and the linear differential operator M is given by (3.14). The operators B and C are symmetric bilinear and trilinear forms, respectively, given by

$$B(X^a,X^b) = \begin{bmatrix} 0 \\ b_1 \\ -\varepsilon b_1 \\ b_2 \\ -\varepsilon b_2 \end{bmatrix}, \quad C(X^a,X^b,X^c) = \begin{bmatrix} 0 \\ c_1 \\ -\varepsilon c_1 \\ c_2 \\ -\varepsilon c_2 \end{bmatrix}.$$

where

$$\begin{aligned} b_1 &= 2W^e v_-^a v_-^b + 2V^e(v_-^a w_-^b + v_-^b w_-^a), \quad b_2 = 2W^e v_+^a v_+^b + 2V^e(v_+^a w_+^b + v_+^b w_+^a), \\ c_1 &= 2v_-^a v_-^b w_-^c + 2v_-^b v_-^c w_-^a + 2v_-^c v_-^a w_-^b, \quad c_2 = 2v_+^a v_+^b w_+^c + 2v_+^b v_+^c w_+^a + 2v_+^c v_+^a w_+^b, \end{aligned}$$

Then

$$\tfrac{1}{2!}B(X,X) = \begin{bmatrix} 0 \\ W^e v_-^2 + V^e v_- w_- \\ -\varepsilon(W^e v_-^2 + V^e v_- w_-) \\ W^e v_+^2 + V^e v_+ w_+ \\ -\varepsilon(W^e v_+^2 + V^e v_+ w_+) \end{bmatrix}, \quad \tfrac{1}{3!}C(X,X,X) = \begin{bmatrix} 0 \\ v_-^2 w_- \\ -\varepsilon v_-^2 w_- \\ v_+^2 w_+ \\ -\varepsilon v_+^2 w_+ \end{bmatrix}.$$

are the quadratic and cubic terms, respectively, of the model system.

At a double Hopf point, the linear operator M has the four critical eigenvalues $\pm i\omega_{1,2}$ on the imaginary axis in the complex plane, and the remaining eigenvalues of M are in the left complex half-plane, bounded away from the imaginary axis. In this situation, for parameter values near the double Hopf point, the nonlinear evolution equation (4.1) possesses a four-dimensional invariant local center manifold W^c_{loc} in the function space H, that is tangent to the critical eigenspace T^c at the double Hopf point. Furthermore, all solutions of (4.1) near the steady state decay exponentially rapidly, as t increases, to the local center manifold W^c_{loc}. Therefore, the local long-term dynamics of the entire system (4.1) is governed by a four-dimensional system of ordinary differential equations that describes the dynamics restricted to W^c_{loc}. In fact, only low-order terms in the Taylor series expansion of this system are required. Finally, a standard procedure of introducing coordinate changes reduces the system of differential equations to a simpler but equivalent one, called a normal form. This normal form is easier to analyze, and predicts the local dynamics of the entire infinite-dimensional system (4.1).

In the Appendix, we give some details of the reduction of the evolution equation (4.1) to the normal form. Our computations are analytical, assisted by the mathematical software package Maple. Near a double Hopf point, the normal form is a four-dimensional system of ordinary differential equations, written in complex notation as

$$\begin{aligned}\dot{\zeta}_1 &= \lambda_1\zeta_1 + G_{2100}\zeta_1^2\bar{\zeta}_1 + G_{1011}\zeta_1\zeta_2\bar{\zeta}_2 + O(\|\mu\|\|\zeta\|^3 + \|\zeta\|^5),\\ \dot{\zeta}_2 &= \lambda_2\zeta_2 + H_{1110}\zeta_1\bar{\zeta}_1\zeta_2 + H_{0021}\zeta_2^2\bar{\zeta}_2 + O(\|\mu\|\|\zeta\|^3 + \|\zeta\|^5),\end{aligned} \tag{4.2}$$

whose solutions $\zeta_1(t)$, $\zeta_2(t)$ are complex numbers that, to leading order, represent the evolving amplitudes and phases of the anti-phase and in-phase oscillatory modes in the nonlinear system (4.1). The critical eigenvalues of the linearization M near the double Hopf point are λ_1 and λ_2, so at the double Hopf point itself we have $\lambda_1 = i\omega_1$, $\lambda_2 = i\omega_2$. Near the double Hopf point, the real parts of the critical eigenvalues $\mu_j = \mathrm{Re}\,\lambda_j$ serve as unfolding parameters that usefully quantify small deviations from the double Hopf point. The higher-order Taylor series terms in the expansions $O(\|\mu\|\|\zeta\|^3 + \|\zeta\|^5)$, where $\mu = (\mu_1, \mu_2)$ and $\zeta = (\zeta_1, \bar{\zeta}_1, \zeta_2, \bar{\zeta}_2)$, are not explicitly needed for our work. The four coefficients G_{jklm} and H_{jklm} of the cubic terms in the normal form are calculated with the help of Maple, for the double Hopf point at parameter values (3.11)–(3.12), and we evaluate them to be

$$\begin{aligned}G_{2100} &= -3.07849 + i0.00166, \qquad & G_{1011} &= -5.89627 + i2.80222,\\ H_{1110} &= -6.00121 - i0.14896, \qquad & H_{0021} &= -2.90063 + i1.38790.\end{aligned} \tag{4.3}$$

The analysis of the normal form (4.2) is described in several textbooks on bifurcation theory. Here we briefly summarize the relevant parts of the treatment in Kuznetsov (2004). If we take polar representations $\zeta_1 = r_1 e^{i\phi_1}$, $\zeta_2 = r_2 e^{i\phi_2}$, and truncate higher-order terms, then in polar coordinates $(r_1, r_2, \phi_1, \phi_2)$ the normal form (4.2) can be written as

$$\begin{aligned}\dot{r_1} &= r_1(\mu_1 + p_{11}r_1^2 + p_{12}r_2^2),\\ \dot{r_2} &= r_2(\mu_2 + p_{21}r_1^2 + p_{22}r_2^2),\\ \dot{\phi}_1 &= \omega_1,\\ \dot{\phi}_2 &= \omega_2,\end{aligned} \tag{4.4}$$

where

$$p_{11} = \mathrm{Re}\,G_{2100}, \quad p_{12} = \mathrm{Re}\,G_{1011}, \quad p_{21} = \mathrm{Re}\,H_{1110}, \quad p_{22} = \mathrm{Re}\,H_{0021}.$$

The truncated normal form (4.4) is an approximation of the normal form (4.2) due to missing higher-order terms in the Taylor series expansions, but for coefficient values (4.3) the approximation is sufficiently accurate to predict the existence and stability of bifurcating solutions. In fact, (4.4) is accurate enough for quantitative comparisons with simulations near the double Hopf point.

We see in the truncated normal form (4.4) that the first pair of equations is independent of the second pair and thus the bifurcations of (4.4) are completely determined by the two equations in r_j, where r_j represent the amplitudes of the anti-phase and in-phase modes:

$$\begin{aligned}\dot{r_1} &= r_1(\mu_1 + p_{11}r_1^2 + p_{12}r_2^2),\\ \dot{r_2} &= r_2(\mu_2 + p_{21}r_1^2 + p_{22}r_2^2).\end{aligned} \tag{4.5}$$

Since we have $p_{11} = -3.07849$ and $p_{22} = -2.90063$, the normal form falls into the "simple" case of Kuznetsov (2004) (p. 359), where $p_{11}p_{22} > 0$ and no fifth-order terms are needed in the amplitude

equations (4.5). Unlike the "difficult" case where $p_{11}p_{22} < 0$, our two-dimensional amplitude equations (4.5) have neither periodic solutions nor codimension-one heteroclinic orbits. Thus the normal form (4.2) is sufficient to predict all the local bifurcations of the model system (2.1)–(2.5) near the double Hopf point at parameter values (3.11)–(3.12). We observe that the system (4.5) has a trivial equilibrium $E_0 = (0,0)$ for all $\mu_{1,2}$. Moreover, there can be as many as three nontrivial equilibria. Equilibria on the coordinate axes

$$E_1 = (r_1, 0),\ r_1 > 0; \qquad E_2 = (0, r_2),\ r_2 > 0,$$

where

$$r_1 = \sqrt{\frac{\mu_1}{-p_{11}}}; \qquad r_2 = \sqrt{\frac{\mu_2}{-p_{22}}}$$

exist if $\mu_1 > 0$, $\mu_2 > 0$, respectively. Another equilibrium

$$E_3 = (r_1, r_2),\ r_1 > 0,\ r_2 > 0,$$

where

$$r_1 = \sqrt{\frac{-\mu_1 + \theta\mu_2}{-p_{11}(\theta\delta - 1)}}, \quad r_2 = \sqrt{\frac{\delta\mu_1 - \mu_2}{-p_{22}(\theta\delta - 1)}}, \tag{4.6}$$

and

$$\theta = \frac{p_{12}}{p_{22}} = 2.03276, \quad \delta = \frac{p_{21}}{p_{11}} = 1.94940, \tag{4.7}$$

exists if both $-\mu_1 + \theta\mu_2 > 0$ and $\delta\mu_1 - \mu_2 > 0$. The equilibria $E_{1,2}$ bifurcate from the origin E_0 at the bifurcation lines

$$H_1 = \{(\mu_1, \mu_2) |\ \mu_1 = 0\}, \quad H_2 = \{(\mu_1, \mu_2) |\ \mu_2 = 0\}, \tag{4.8}$$

and E_3 bifurcates from E_2 or E_1 on the bifurcation lines

$$\begin{aligned} T_1 &= \{(\mu_1, \mu_2) |\ \mu_1 = \theta\mu_2,\ \mu_2 > 0\}, \\ T_2 &= \{(\mu_1, \mu_2) |\ \mu_2 = \delta\mu_1,\ \mu_1 > 0\}, \end{aligned} \tag{4.9}$$

respectively. We plot the parametric portraits of (4.5) in Figure 2. In the left panel, the four lines H_1, H_2, T_1 and T_2 divide the (μ_1, μ_2) parameter plane into six regions. In region I, the amplitude system (4.5) has the unique equilibrium E_0 and it is asymptotically stable. When entering region II (or VI) from region I, the equilibrium E_1 (or E_2) bifurcates from E_0 and is asymptotically stable, while E_0 is unstable. When entering region III (or V) from region II (or VI), another, unstable, equilibrium E_2 (or E_1) bifurcates from E_0 while E_1 (or E_2) remains asymptotically stable and E_0 is unstable. Finally, in region IV, there is bistability as the two equilibria E_1 and E_2 are both asymptotically stable. A fourth equilibrium E_3 exists and is unstable, while E_0 is unstable. Although E_3 is unstable, it has an important effect on the overall dynamics. The unstable manifold of E_3 forms the boundary between the basins of attraction of the two stable equilibria E_1 and E_2. Thus the eventual limiting state of a generic trajectory depends on the location of its initial value relative to the unstable manifold of E_3. For more details, including phase portraits, see Kuznetsov (2004). If we fix other parameters and only change β or D near the double Hopf point, the curves corresponding to H_j, T_j in the (β, D) plane are shown in the right panel of Figure 2.

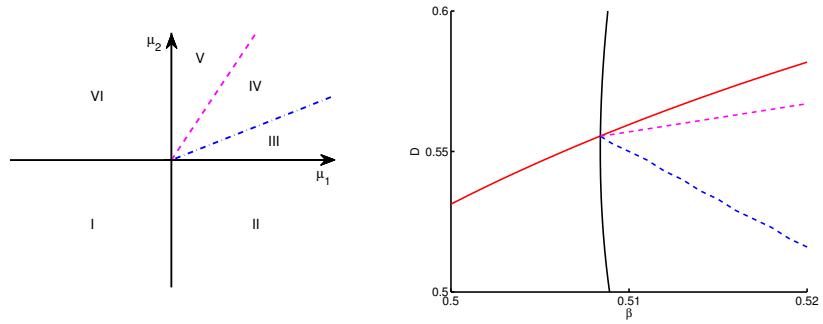

FIG. 2. Parametric portrait of the amplitude equations (4.5) in the (μ_1,μ_2) plane (left panel) and the corresponding portrait in the (β,D) plane (right panel). In the left panel, the magenta dashed line is $T_2:\mu_2=\delta\mu_1$ and the blue dashed line is $T_1:\mu_1=\theta\mu_2$. In the right panel, the black curve corresponds to the μ_1-axis $H_2:\mu_2=0$ in the (μ_1,μ_2) plane, the red curve corresponds to the μ_2-axis $H_1:\mu_1=0$, the magenta dashed curve corresponds to T_2 and the blue dashed curve corresponds to T_1.

The solid black curve corresponds to the μ_1-axis H_2, and the solid red curve corresponds to the μ_2-axis H_1. The dashed curves are linear approximations of the curves corresponding to the T_j.

Restoring the angular variables to (4.5) to recover the truncated normal form (4.4), the equilibria of the amplitude equations (4.5) receive different interpretations. The origin E_0 is still an equilibrium at the origin, but E_1 and E_2 are limit cycles, or isolated periodic solutions of (4.4), while E_3 for (4.4) is a two-dimensional invariant torus. Their stability properties remain the same. Thus the lines H_j correspond to Hopf bifurcations, and the lines T_j to torus (or Neimark-Sacker) bifurcations.

Because nondegeneracy conditions are satisfied in our case, restoring the higher-order terms to the truncated normal form (4.4) to return to (4.2) changes the bifurcation results only subtly. The torus bifurcation lines T_j become torus bifurcation curves $T_1:\mu_1=\theta\mu_2+O(\mu_2^2)$ and $T_2:\mu_2=\delta\mu_1+O(\mu_1^2)$ tangent at the origin to the lines (4.9), while solutions restricted to the invariant two-torus are slightly changed, but the two-torus itself persists as a normally hyperbolic invariant manifold with the same stability type.

Finally, transferring the bifurcation and stability results to the original model system (4.1), or equivalently (2.1)–(2.5), is straightforward. The origin E_0 corresponds to the steady state (3.1), E_1 and E_2 correspond to nonlinear oscillating anti-phase and in-phase modes, and E_3 corresponds to an invariant two-torus or modulated oscillations, while the stability types remain the same. Solutions on the invariant two-torus are characterized by two frequencies, one near ω_1 and the other near ω_2.

To check our results we consider parameter paths near the double Hopf point in the (β,D) plane and plot corresponding bifurcation diagrams obtained by using AUTO on a spatially discretized finite-difference approximation of the model system (2.1)–(2.5). In Figure 3, we consider a parameter path where we fix $D=0.54$ and increase β from 0.50 to 0.52. This parameter path is shown in green in the inset panel of the figure. The starting point is to the left of the two Hopf bifurcation curves, and as β increases the parameter path crosses the red (anti-phase) Hopf bifurcation curve, then the black (in-phase) Hopf bifurcation curve, and finally the dashed blue torus bifurcation curve. In the main part of Figure 3 we show the bifurcation diagram plotted by AUTO for the finite-difference approximation of the model system, where β is plotted along the horizontal axis, V_- along the vertical. Moving rightwards from the left edge of the diagram ($\beta=0.50$), there is a Hopf bifurcation from the steady state to asymptotically stable anti-phase oscillating modes (solid circles), then another Hopf bifurcation

from the steady state to unstable in-phase oscillating modes (open circles). As β increases further, the in-phase modes gain stability as the parameter values enter a region of bistability, with asymptotically stable anti-phase and in-phase modes coexisting. AUTO indicates that when the in-phase modes gain stability, a pair of complex conjugate Floquet multipliers of the in-phase modes cross inside the unit circle in the complex plane, which is characteristic of a torus bifurcation. This is all qualitatively consistent with the dynamics predicted by the parameter path in the (β, D) plane crossing the bifurcation curves obtained from the amplitude equations (4.5). Although both the amplitude equations (due to truncation of higher-order terms) and the AUTO bifurcation computations (due to finite differences) are approximations of the model system, the numerical values of the bifurcation points agree well, close to the double Hopf point.

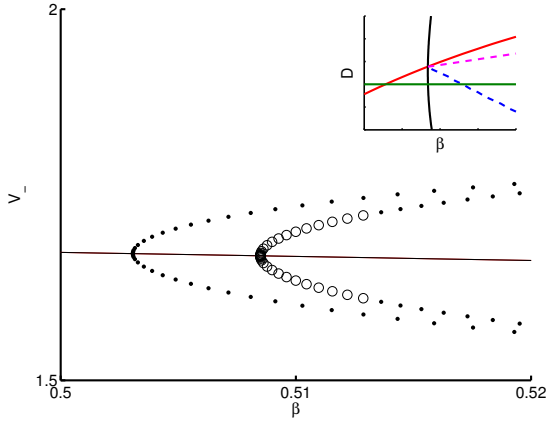

FIG. 3. Bifurcation diagram for the model system, with $D = 0.54$ fixed and β increasing from 0.50 to 0.52. The inset panel shows the parameter path plotted in green in the (β, D) plane, together with the bifurcation curves obtained from the normal form. As β increases (moving to the right on the green path), the parameter path crosses the solid red Hopf bifurcation curve for anti-phase modes, the solid black Hopf bifurcation curve for in-phase modes, and the dashed blue torus bifurcation curve. The main panel shows the bifurcation diagram for the parameter path obtained using AUTO on a spatially discretized finite-difference approximation of the model system, with β plotted on the horizontal axis, the v_- component of the vector solution on the vertical axis.

Similarly, in Figure 4 we consider a parameter path fixing $\beta = 0.509$ and incresing D from 0.5 to 0.6. This parameter path is shown in green in the inset panel. As D increases, the parameter path crosses the dashed blue torus bifurcation curve, the dashed magenta torus bifurcation curve, and the solid red Hopf bifurcation curve. The main panel shows the bifurcation diagram obtained by AUTO. As D increases, the in-phase mode remains near the steady state and changes stability from unstable to asymptotically stable. The anti-phase mode starts asymptotically stable with a large amplitude. As D increases the amplitude shrinks, the anti-phase mode becomes unstable, then it disappears in a Hopf bifurcation at the steady state. Again the sequence of stability changes and bifurcations is as predicted by the normal form analysis, and there is good agreement between the numerical values of the bifurcation points.

AUTO is able to detect stability changes of periodic solutions that correspond to torus bifurcations, but is unable to continue along branches of invariant tori. To look for invariant tori where their existence is predicted by the normal form analysis, we simulated directly the model system (2.1)–(2.5) with finite differences in both space and time. Although the tori are unstable, if initial conditions are chosen close enough to an invariant torus, the solution will stay close to a solution on the unstable torus for some time

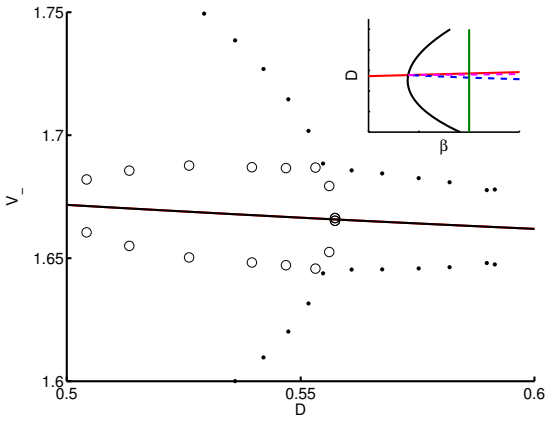

FIG. 4. Bifurcation diagram for the model system, with $\beta = 0.509$ fixed and D increasing from 0.50 to 0.60. The inset panel shows the parameter path plotted in green in the (β, D) plane, together with the bifurcation curves obtained from the normal form. As D increases (moving upwards on the green path), the parameter path crosses the dashed blue torus bifurcation curve, the dashed magenta torus bifurcation curve, and the solid red Hopf bifurcation curve for anti-phase modes. The main panel shows the bifurcation diagram for the parameter path obtained using AUTO on a spatially discretized finite-difference approximation of the model system, with D plotted on the horizontal axis, the v_- component of the vector solution on the vertical axis.

before the exponentially growing drift apart becomes noticeable. We take $\beta = 0.509$ and $D = 0.55486$, which, according to the normal form, is in the parameter region between the two torus bifurcation curves, where there is bistability due to both the anti-phase and in-phase modes being asymptotically stable, and an unstable invariant torus. We choose the initial condition corresponding to

$$X(0) = \mathrm{Re}(r_1 q_1 + r_2 q_2), \tag{4.10}$$

recalling that the vector $X(t)$ represents the deviation of variables from the steady state (3.1), and r_1, r_2 are the amplitudes (4.6)–(4.7) given by the equilibrium E_3 of the amplitude equations that corresponds to the invariant torus. Since the parameters are close to the double Hopf point, we reason that neglect of higher-order terms in the amplitude equations and in the local center manifold should not give seriously large errors, and therefore (4.10) represents an initial condition close to the unstable invariant torus. The simulated results appear to validate this choice of initial condition. A plot of the time evolution of V_- component of the solution is shown in the left panel of Figure 5. For a reasonably long time the numerical solution exhibits oscillations characterized by two periods which correspond to the two oscillating frequencies ω_1 and ω_2 at the double Hopf point. The signal displays a phenomenon similar to that of beats or amplitude modulation that occurs when two linear oscillations with nearly the same frequencies are added, with a fast "carrier" frequency $|\omega_1 + \omega_2|$ and a slow modulated "envelope" frequency $|\omega_1 - \omega_2|$. The power spectrum from an FFT analysis of the time series of the numerical solution is shown in the right panel of Figure 5. The two peaks on the FFT plot indicate the two main frequency components from the time series in the left panel, and the peak locations on the horizontal axis agree with the values of ω_1, ω_2. This is consistent with the predictions of the normal form analysis.

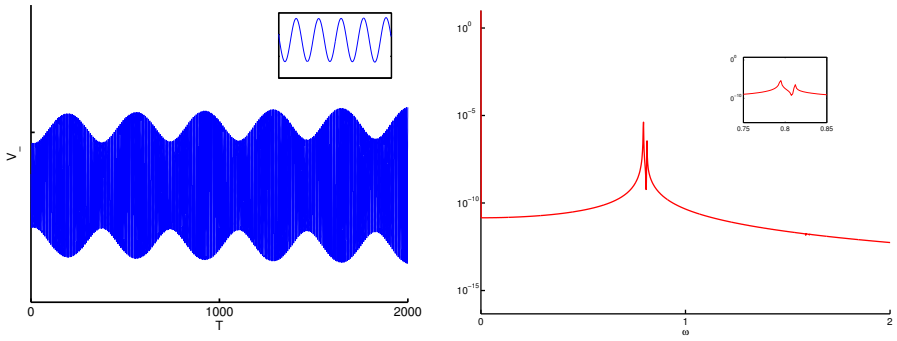

FIG. 5. The time evolution of the V_- component of a simulated solution of the model system with initial condition (4.10) (left) and its corresponding power spectrum obtained from FFT analysis (right). In the left panel, we can observe two periods from the series. The shorter period corresponds to angular frequency $|\omega_1 + \omega_2|$ and the longer period corresponds to angular frequency $|\omega_1 - \omega_2|$. The left inset panel shows the simulation results on a short time scale that more clearly resolves the rapid oscillations corresponding to the shorter period. In the right panel, the power spectrum of the solution is plotted, where the horizontal axis is angular frequency ω. Two peaks in the power spectrum at $\omega = 0.79$ and $\omega = 0.81$ are clearly visible. The inset in the right panel shows more detail near $\omega = 0.8$.

5. Discussion

We have studied a model of two identical compartments, represented by chemical oscillators with Sel'kov kinetics, coupled by a chemical signal that diffuses and degrades in a one-dimensional bulk medium. Previous numerical work on this model system of partial and ordinary differential equations showed the presence of two modes of synchronized oscillations, in-phase and anti-phase, that arise through Hopf bifurcations from the steady state. The pattern of Hopf bifurcations and stability of the modes suggested the existence of an invariant torus in the dynamics. In this paper we use center manifold and normal form theory to reduce the local dynamics of the model system to a normal form for a double Hopf bifurcation, which predict configurations of Hopf bifurcations and stability of the in-phase and anti-phase modes near the double Hopf point. The nomal form also shows the existence of an unstable invariant torus in the dynamics of the model system, and the location of the torus and its stable manifold can be approximated from the normal form near the double Hopf point. For the parameter values we studied, but with no coupling ($\beta = 0$), the compartments (2.3) and (2.4) have only unique globally asymptotically stable steady states. Thus the oscillators are conditional and coupling through the bulk is necessary for the oscillations. The predictions of the normal form are checked with numerical simulations and continuation-bifurcation computations with the spatially discretized model. We note that the reduction to the normal form is analytical, working with the continuum system itself with no spatial discretization.

In the study of coupled oscillators, double Hopf bifurcations often appear in delay-coupled systems, e.g. (Buono & Bélair, 2003; Shayer & Campbell, 2000). In our model, there is no explicit delay term, but the communication between the two oscillators is through spatial diffusion of a signalling chemical in the bulk medium. For spatially separated compartments, this can be a more realistic way to describe the connections among individuals and at the same time diffusion serves effectively as a time delay, reflecting the time needed for a chemical to change concentration at a distant location. In fact, diffusion can be represented as a distributed delay through the variation of constants formula (Busenberg &

Mahaffy, 1985), and this sometimes has practical advantages.

Since the two oscillators we considered are identical and the coupling is symmetric, from a symmetry point of view the existence of an anti-phase mode of synchrony is not surprising. Many other works have noted the existence of a stable anti-phase synchrony in pairs of identical coupled oscillators, see e.g. Sherman (1994) and references therein. Coupling by bulk diffusion, in a model similar to the one studied in this paper, is considered by Gomez-Marin et al. (2007), and Gou & Ward (2015), where anti-phase synchrony is found. The interaction of in-phase and anti-phase modes is often explored by simulation, or with numerical continuation and bifurcation programs such as AUTO. At a double Hopf bifurcation, it is possible to analytically determine the stability of both the in-phase and anti-phase modes and their interactions near the organizing center of a double Hopf point. This organizing center provides a useful point of reference for a more global study using numerical continuation and simulation (Gou et al., 2015a). Also, the double Hopf normal form could provide starting values for numerical torus continuations, and the stable manifolds of these tori would give global information on the basin boundaries of competing attractors in bistable cases. Since the double Hopf bifurcation is structurally stable, it is not necessary for the two coupled compartments to be exactly identical: a pair of sufficiently similar compartments coupled nearly symmetrically in the bulk will have qualitatively the same dynamics. Thus, nonsymmetric systems can have anti-phase and in-phase synchronies that interact similarly to the synchronies in the model studied here.

We studied the simplest coupled system with two compartments. In systems with N coupled compartments, $N > 2$, there also can exist stable in-phase and anti-phase synchronies, possibly coexisting, e.g. (Gonze et al., 2008; Merriam et al., 2005; Schroder et al., 2012). Anti-phase synchronies appear between groupings of compartments, which may be imposed by assigning different coupling strengths, or may emerge spontaneously when coupling is symmetric. A double Hopf bifurcation analysis could be used to explore the interactions between such in-phase and anti-phase synchronies, if we restrict dynamics to a symmetric invariant subspace. However, for an N-compartment system there exist other synchronies. It would be interesting to investigate cases where a collection of N compartments are evenly spaced in a finite or infinite one-dimensional domain, where we could expect synchronized oscillation modes in addition in-phase and anti-phase. To fully determine all existing sychronies, together with their stability and interactions, in a given N-compartment system would be a substantial undertaking for moderately large values of N, but a good starting point would be to use a general algebraic formalism (Golubitsky & Stewart, 2006) that depends only on coupling configurations, to first determine the synchronies to investigate.

The current study has examined synchrony in a one-dimensional bulk region with two spatially separated compartments. Another natural progression of this work is to extend the model into a two- or three-dimensional bulk region. In a higher dimensional bulk region, with possible constraints such as symmetric cell locations, a limited number of analytical tools could be used to obtain some insight into spatio-temporal pattern formation. Moreover, the present model only considers linear coupling, where the influence of the signalling chemical on the regulation mechanism is proportional to its concentration. Simple Hopf bifurcations of in-phase synchronies with nonlinear coupling are considered by Gou et al. (2015b). A worthwhile study would be to consider a different coupling mechanisms such as those suggested in experiments with *Dictyostelium* ameobae (Winfree, 2010) and compare how different synchronies interact.

A. Calculation of normal form coefficients

In this Appendix, we describe the calculations to evaluate the four cubic coefficients G_{jklm}, H_{jklm} in the normal form (4.2) that governs the dynamics near a double Hopf point. To evaluate the cubic coefficients, it is sufficient to take parameters at the double Hopf point, thus $\mu_1 = \mu_2 = 0$ and we have

$$\begin{aligned} \dot{\zeta}_1 &= i\omega_1\zeta_1 + G_{2100}\zeta_1^2\bar{\zeta}_1 + G_{1011}\zeta_1\zeta_2\bar{\zeta}_2 + O(\|(\zeta_1,\bar{\zeta}_1,\zeta_2,\bar{\zeta}_2)\|^5), \\ \dot{\zeta}_2 &= i\omega_2\zeta_2 + H_{1110}\zeta_1\bar{\zeta}_1\zeta_2 + H_{0021}\zeta_2^2\bar{\zeta}_2 + O(\|(\zeta_1,\bar{\zeta}_1,\zeta_2,\bar{\zeta}_2)\|^5). \end{aligned} \tag{A.1}$$

At the double Hopf point, the nonlinear system (3.2)–(3.3), written as (4.1), is reduced to a system on a four-dimensional center manifold that is tangent, in the infinite-dimensional function space H, to the critical eigenspace T^c. Since this center manifold reduction is standard and follows closely the analogous procedure at a simple Hopf bifurcation described in detail for reaction-diffusion systems in the textbook of Kuznetsov (2004), we give only a short description together with some details specific to our system. This center manifold system is further reduced to the normal form (A.1).

We first construct a projection P^c of the space H, onto the critical eigenspace T^c. This requires an inner product, and two adjoint eigenvectors. For a pair of complex vectors

$$p = \begin{bmatrix} \xi(x) \\ \chi_- \\ \vartheta_- \\ \chi_+ \\ \vartheta_+ \end{bmatrix}, \quad q = \begin{bmatrix} \eta(x) \\ \varphi_- \\ \psi_- \\ \varphi_+ \\ \psi_+ \end{bmatrix},$$

we define their inner product to be

$$\langle p,q\rangle = \int_{-L}^{+L} \overline{\xi(x)}\eta(x)\,dx + \overline{\chi}_-\varphi_- + \overline{\vartheta}_-\psi_- + \overline{\chi}_+\varphi_+ + \overline{\vartheta}_+\psi_+.$$

With respect to this inner product, the adjoint to the linear differential operator M is the linear differential operator M^*, given by

$$M^*\begin{bmatrix} \xi(x) \\ \chi_- \\ \vartheta_- \\ \chi_+ \\ \vartheta_+ \end{bmatrix} = \begin{bmatrix} D\xi''(x) - k\xi(x) \\ f_V\chi_- + \varepsilon g_V\vartheta_- - \beta\chi_- + \kappa\xi(-L) \\ f_W\chi_- + \varepsilon g_W\vartheta_- \\ f_V\chi_+ + \varepsilon g_V\vartheta_+ - \beta\chi_+ + \kappa\xi(+L) \\ f_W\chi_+ + \varepsilon g_W\vartheta_+ \end{bmatrix},$$

with adjoint boundary conditions

$$\begin{aligned} -D\xi(-L) &= \beta\chi_- - \kappa\xi(-L), \\ +D\xi(+L) &= \beta\chi_+ - \kappa\xi(+L). \end{aligned}$$

We solve for two adjoint eigenvectors

$$p_j = \begin{bmatrix} \xi_j(x) \\ \chi_{j,-} \\ \vartheta_{j,-} \\ \chi_{j,+} \\ \vartheta_{j,+} \end{bmatrix},$$

$j = 1, 2$, satisfying

$$M^* p_1 = -i\omega_1 p_1, \qquad M^* p_2 = -i\omega_2 p_2,$$

with normalizations such that

$$\langle p_1, q_1 \rangle = 1, \qquad \langle p_2, q_2 \rangle = 1, \tag{A.2}$$

where q_1, q_2 are the eigenvectors given in Section 3. We note that orthogonality conditions

$$\begin{aligned} &\langle p_1, q_2 \rangle = 0, \quad \langle p_1, \overline{q}_1 \rangle = 0, \quad \langle p_1, \overline{q}_2 \rangle = 0 \\ &\langle p_2, q_1 \rangle = 0, \quad \langle p_2, \overline{q}_1 \rangle = 0, \quad \langle p_2, \overline{q}_2 \rangle = 0, \end{aligned}$$

are automatically satisfied. We obtain

$$p_1 = a_1^0 \begin{bmatrix} \xi_{10} \sinh \Omega_3 x / \sinh \Omega_3 L \\ -1 \\ f_w/(i\omega_1 + \varepsilon g_w) \\ 1 \\ -f_w/(i\omega_1 + \varepsilon g_w) \end{bmatrix}, \quad p_2 = a_2^0 \begin{bmatrix} \xi_{20} \cosh \Omega_4 x / \cosh \Omega_4 L \\ 1 \\ -f_w/(i\omega_2 + \varepsilon g_w) \\ 1 \\ -f_w/(i\omega_2 + \varepsilon g_w) \end{bmatrix},$$

where the constants

$$a_1^0 = 0.250508 - i0.172379, \qquad a_2^0 = 0.253847 - i0.181974,$$

are chosen so that the normalization conditions (A.2) hold, and

$$\Omega_3 = \sqrt{\tfrac{k - i\omega_1}{D}}, \quad \Omega_4 = \sqrt{\tfrac{i - i\omega_2}{D}}, \quad \xi_{10} = \tfrac{\beta}{\kappa + D\Omega_3 \coth \Omega_3 L}, \quad \xi_{20} = \tfrac{\beta}{\kappa + D\Omega_4 \tanh \Omega_4 L}.$$

We define the projection P^c, of H onto the critical eigenspace T^c, by

$$P^c X = z_1 q_1 + \bar{z}_1 \overline{q}_1 + z_2 q_2 + \bar{z}_2 \overline{q}_2,$$

for any $X \in H$, where z_1, z_2 are complex numbers given by the inner products

$$z_1 = \langle p_1, X \rangle, \qquad z_2 = \langle p_2, X \rangle.$$

Now we can use the projection P^c to split any vector $X \in H$ into two parts

$$X = X^c + Y,$$

where the "center" part

$$X^c = P^c X = z_1 q_1 + \bar{z}_1 \overline{q}_1 + z_2 q_2 + \bar{z}_2 \overline{q}_2$$

belongs to the four-dimensional critical eigenspace T^c and the complementary part

$$Y = (I - P^c)X = X - \langle p_1, X \rangle q_1 - \langle \overline{p}_1, X \rangle \overline{q}_1 - \langle p_2, X \rangle q_2 - \langle \overline{p}_2, X \rangle \overline{q}_2,$$

where I denotes the identity operator, belongs to the infinite-dimensional stable subspace T^s. Correspondingly, the system (4.1) splits into two parts

$$\dot{X}^c = MX^c + \tfrac{1}{2} P^c B(X^c + Y, X^c + Y) + \tfrac{1}{6} P^c C(X^c + Y, X^c + Y, X^c + Y), \tag{A.3}$$

$$\dot{Y} = MY + \tfrac{1}{2}(I-P^c)B(X^c+Y,X^c+Y) + \tfrac{1}{6}(I-P^c)C(X^c+Y,X^c+Y,X^c+Y). \tag{A.4}$$

By center manifold theory, there is an invariant, exponentially attracting, four-dimensional local center manifold in H that is tangent to the critical eigenspace T^c, and the center manifold can be expanded in a Taylor series as

$$Y = Y(z_1,\bar{z}_1,z_2,\bar{z}_2) = \sum_{j+k+l+m=2} \tfrac{1}{j!k!l!m!} w_{jklm} z_1^j \bar{z}_1^k z_2^l \bar{z}_2^m + O(\|(z_1,\bar{z}_1,z_2,\bar{z}_2)\|^3). \tag{A.5}$$

Substituting the expansion (A.5) into (A.3)–(A.4) and using the invariance of the center manifold, we collect terms of like powers and obtain nonhomogeneous linear boundary value problems for each of the ten coefficient vectors w_{jklm} at second order ($j+k+l+m=2$; $j,k,l,m \geqslant 0$),

$$\begin{aligned}
(2i\omega_1 I - M)w_{2000} &= (I-P^c)B(q_1,q_1),\\
-Mw_{1100} &= (I-P^c)B(q_1,\bar{q}_1),\\
(i\omega_1 I + i\omega_2 I - M)w_{1010} &= (I-P^c)B(q_1,q_2),\\
(i\omega_1 I - i\omega_2 I - M)w_{1001} &= (I-P^c)B(q_1,\bar{q}_2),\\
&\text{etc.}
\end{aligned}$$

Using the explicit expressions (3.17) for q_1 and q_2, we use matrix algebra and the method of undetermined coefficients, assisted by the mathematical software package Maple, to solve for the w_{jklm} that we require. It is helpful to use symmetry to reduce the number of explicit solutions needed.

Substituting (A.5) into each of the components of (A.3), we obtain a four-dimensional ordinary differential equation that gives the dynamics restricted to the invariant local center manifold,

$$\begin{aligned}
\dot{z}_1 &= i\omega_1 z_1 + g(z_1,\bar{z}_1,z_2,\bar{z}_2),\\
\dot{z}_2 &= i\omega_2 z_2 + h(z_1,\bar{z}_1,z_2,\bar{z}_2).
\end{aligned} \tag{A.6}$$

Expanding in Taylor series

$$\begin{aligned}
g(z_1,\bar{z}_1,z_2,\bar{z}_2) &= \sum_{j+k+l+m\geqslant 2} g_{jklm} z_1^j \bar{z}_1^k z_2^l \bar{z}_2^m,\\
h(z_1,\bar{z}_1,z_2,\bar{z}_2) &= \sum_{j+k+l+m\geqslant 2} h_{jklm} z_1^j \bar{z}_1^k z_2^l \bar{z}_2^m,
\end{aligned}$$

the ten quadratic coefficients of the center manifold system (A.6) are given by

$$\begin{aligned}
g_{2000} &= \tfrac{1}{2}\langle p_1, B(q_1,q_1)\rangle,\\
g_{1100} &= \langle p_1, B(q_1,\bar{q}_1)\rangle,\\
g_{1010} &= \langle p_1, B(q_1,q_2)\rangle,\\
g_{1001} &= \langle p_1, B(q_1,\bar{q}_2)\rangle,\\
&\text{etc.}
\end{aligned}$$

Note that several of these coefficients vanish due to symmetry. We need explicitly only four of the cubic coefficients of the centre manifold system (A.6),

$$\begin{aligned}
g_{2100} &= \langle p_1, B(q_1,w_{1100}) + \tfrac{1}{2}B(\bar{q}_1,w_{2000}) + \tfrac{1}{2}C(q_1,q_1,\bar{q}_1)\rangle,\\
g_{1011} &= \langle p_1, B(q_1,w_{0011}) + B(q_2,w_{1001}) + B(\bar{q}_2,w_{1010}) + C(q_1,q_2,\bar{q}_2)\rangle,\\
h_{1110} &= \langle p_2, B(q_2,w_{1100}) + B(q_1,w_{0110}) + B(\bar{q}_1,w_{1010}) + C(q_1,\bar{q}_1,q_2)\rangle,\\
h_{0021} &= \langle p_2, B(q_2,w_{0011}) + \tfrac{1}{2}B(\bar{q}_2,w_{0020}) + \tfrac{1}{2}C(q_2,q_2,\bar{q}_2)\rangle.
\end{aligned}$$

Finally, a near-identity coordinate transformation of the form

$$z_1 = \zeta_1 + O(\|(\zeta_1, \bar{\zeta}_1, \zeta_2, \bar{\zeta}_2)\|^2), \quad z_2 = \zeta_2 + O(\|(\zeta_1, \bar{\zeta}_1, \zeta_2, \bar{\zeta}_2)\|^2),$$

takes the the center manifold system (A.6) into the normal form (A.1). The procedure to construct the coordinate transformation is lengthy but standard, and is described in textbooks. For example, see Kuznetsov (2004) for more details. In the end, there are formulas derived for the cubic coefficients in the normal form (A.1), in terms of the quadratic and cubic coefficients of the center manifold system (A.6): see equations (8.90)–(8.93) in Kuznetsov (2004). We use Maple to evaluate these coefficients numerically, obtaining (4.3).

REFERENCES

Buono, P. & Bélair, J. (2003) Restrictions and unfolding of double Hopf bifurcation in functional differential equations. *J. Diff. Equ.*, **189**, 234–266.

Busenberg, S. & Mahaffy, J. (1985) Interaction of spatial diffusion and delays in models of genetic control by repression. *J. Math. Biol.*, **22**, 313–333.

Chiang, W. Y., Li, Y. X. & Lai, P. Y. (2011) Simple models for quorum sensing: Nonlinear dynamical analysis. *Phys. Rev. E*, **84**, 041921.

Chou, T. & D'Orsogna, M. (2007) Multistage adsorption of diffusing macromolecules and viruses. *J. Chem. Phys.*, **127**, 105101.

De Monte, S., d'Ovidio, F., Danø, S. & Sørensen, P. (2007) Dynamical quorum sensing: Population density encoded in cellular dynamics. *Proc. Nat. Acad. Sci. USA*, **104**, 18377–18381.

Doedel, E., Champneys, A., Fairgreave, T., Kuznetsov, Y., Sandstede, B. & Wang, X. (1997) AUTO97: Continuation and Bifurcation Software for Ordinary Differential Equations (with HomCont). Technical report, Concordia Univ., Montreal.

Ermentrout, B. (2002) *Simulating, Analyzing, and Animating Dynamical Systems: A Guide to XPPAUT for Researchers and Students*. SIAM, Philadelphia.

Goldbeter, A. (1990) *Biochemical Oscillations and Cellular Rhythms: The Molecular Bases of Periodic and Chaotic Behaviour*. Cambridge University Press, Cambridge.

Golubitsky, M. & Stewart, I. (2006) Nonlinear dynamics of networks: The groupoid formalism. *Bull. AMS*, **43**, 305–364.

Gomez-Marin, A., Garcia-Ojalvo, J. & Sancho, J. (2007) Self-sustained spatiotemporal oscillations induced by membrane-bulk coupling. *Phys. Rev. Lett.*, **98**, 168303.

Gonze, D., Markadieu, N. & Goldbeter, A. (2008) Selection of in-phase or out-of-phase synchronization in a model based on global coupling of cells undergoing metabolic oscillations. *Chaos*, **18**, 037127.

Gou, J., Chiang, W., Lai, P., Ward, M. & Li, Y. (2015a) A theory of synchrony by coupling through a diffusive chemical signal. Submitted to Physica D.

Gou, J., Li, Y., Nagata, W. & Ward, M. (2015b) Synchronized oscillatory dynamics for a 1-d model of membrane kinetics coupled by bulk diffusion. Submitted to SIAM J. Appl. Dyn. Syst.

Gou, J. & Ward, M. (2015) Oscillatory dynamics for a coupled membrane-bulk diffusion model with Fitzhugh-Nagumo membrane kinetics. Submitted to SIAM J. Appl. Math.

Knobil, E. (1974) On the control of gonadotropin secretion in the rhesus monkey. *Rec. Prog. Horm. Res.*, **30**, 1–46.

Kuznetsov, Y. (2004) *Elements of Applied Bifurcation Theory*. Springer, New York.

Li, Y. & Khadra, A. (2008) Robust synchrony and rhythmogenesis in endocrine neurons *via* autocrine regulation *in vitro* and *in vivo*. *Bull. Math. Biol.*, **70**, 2103–2125.

MacDonald, P. & Rorsman, P. (2006) Oscillations, intercellular coupling, and insulin secretion in pancreatic β cells. *PLoS Biol.*, **4**, 167–171.

Merriam, E., Netoff, T. & Banks, M. (2005) Bistable network behavior of layer I interneurons in auditory cortex. *The Journal of Neuroscience*, **25**, 6175–6186.

Miller, M. & Bassler, B. (2001) Quorum sensing in bacteria. *Ann. Rev. Microbiol.*, **55**, 165–199.

Müller, J., Kuttler, C., Hense, B., Rothballer, M. & Hartmann, A. (2006) Cell-cell communication by quorum sensing and dimension-reduction. *J. Math. Biol.*, **53**, 672–702.

Müller, J. & Uecker, H. (2013) Approximating the dynamics of communicating cells in a diffusive medium by ODEs – homogenization with localization. *J. Math. Biol.*, **67**, 1023–1065.

Schroder, S., Herzog, E. & Kiss, I. (2012) Transcription-based oscillator model for light-induced splitting as antiphase circadian gene expression in the suprachiasmatic nuclei. *J. Biol. Rhythms*, **27**, 79–90.

Segota, I., Boulet, L., Franck, D. & Franck, C. (2014) Spontaneous emergence of large-scale cell cycle synchro-

nization in amoeba colonies. *Phys. Biol.*, **11**, 036001.

Shayer, L. & Campbell, S. (2000) Stability, bifurcation, and multistability in a system of two coupled neurons with multiple time delays. *SIAM J. Appl. Math.*, **61**, 673–700.

Sherman, A. (1994) Anti-phase, asymmetric and aperiodic oscillations in excitable cells–I. Coupled bursters. *Bull. Math. Biol.*, **56**, 811–835.

Shvartsman, S., Shütz, E., Imbihl, R. & Kevrekidis, I. (1999) Dynamics on microcomposite catalytic surfaces: The effect of active boundaries. *Phys. Rev. Lett.*, **83**(14), 2857–2860.

Varela, F., Lachaux, J., Rodriguez, E. & Martinerie, J. (2001) The brainweb: Phase synchronization and large-scale integration. *Nature Rev. Neurosci.*, **2**, 229–239.

Winfree, A. (2010) *The Geometry of Biological Time*. Springer, New York.